Acta Cryst. (1996). B52, 72–77

Structure of Ferroelectric $Pb_5Al_3F_{19}$ at 160 K, Polarization Reversal and Relationship to Ferroelectric $Pb_5Cr_3F_{19}$ at 295 K

S. SARRAUTE,[a] J. RAVEZ,[a] R. VON DER MÜHLL,[a] G. BRAVIC,[b] R. S. FEIGELSON[c] AND S. C. ABRAHAMS[d]

[a]*Institut de Chimie de la Matière Condensée de Bordeaux, Chateau Brivazac, F-33600 Pessac, France,* [b]*Laboratoire de Cristallographie et de Physique Cristalline, Université Bordeaux I, F-33405 Talence, France,* [c]*Center for Materials Research, Stanford University, Stanford, CA 94305, USA, and* [d]*Physics Department, Southern Oregon State College, Ashland, OR 97520, USA*

(*Received 8 February 1995; accepted 21 June 1995*)

Abstract

$Pb_5Al_3F_{19}$ at 160 K is ferroelectric, crystallizing in the tetragonal system. With $M_r = 1477.9$, the space group is *I*4*cm* and $a = 14.07(2)$, $c = 7.30(1)$ Å, $V = 1445(3)$ Å^3, $Z = 4$, $D_x = 6.793$ Mg m^{-3}. For λ(Mo $K\alpha$) = 0.71073 Å, $\mu = 56.36$ mm^{-1}. $F(000) = 2480$. $Pb_5Al_3F_{19}$ undergoes a first-order phase transition on cooling at 120 K and on heating at 270 K. The structure was determined from 656 independent $F(hkl)$ with $I > 3\sigma(I)$ and refined by least squares to $R = 0.0527$, $wR = 0.0480$, $S = 1.065$. No atom is further than 0.83 Å from the hypothetical *I*4/*mcm* atomic positions, hence the crystal is structurally ferroelectric. The mean atomic polar displacement of the two independent Al atoms from the zero spontaneous-polarization location, allowing for the F atoms, is 0.207(28) Å which leads to a predicted $T_c = 860(230)$ K. Several additional phase transitions are known to form before the hypothetical phase is attained. Each independent Al atom occupies a fluorine octahedron with average Al—F distance either 1.818(5) or 1.824(1) Å. One Pb atom is nine coordinated, occupying a distorted tricapped trigonal prism with average Pb—F = 2.66(22) Å. The other is ten coordinated, forming a distorted bicapped cuboid, with average Pb—F = 2.61(28) Å. Pyroelectric pulses are readily detectable in crystals cooled below 120 K, or subsequently on heating to 270 K. Similarly, numerous piezoelectric resonances are observed in the same thermal ranges; the compression mode at ~1197 kHz has been identified by its characteristic admittance circle. The mechanical quality factor Q_m for ferroelectric $Pb_5Al_3F_{19}$, determined from the admittance-circle-derived equivalent circuit, is ~423.

1. Introduction

An increasing number of complex fluorides containing fluorine octahedra have recently been shown to exhibit ferroelectricity, see Abrahams & Ravez (1992) and Ravez (1985, 1986) for reviews. Among these are the AMF_5 family, with A = Sr, M = Al, Cr, Ga; A = Ba, M = Ti, V, Fe, and the $Pb_3M_2F_{12}$ family, with M = Al, Ti, V, Cr, Fe, Ga (see reviews above, also Moulton & Feigelson, 1991), in addition to the $Pb_5M_3F_{19}$ family, with M = Al, Ti, V, Cr, Fe, Ga (Ravez, Andriamampianina, Simon, Grannec & Abrahams, 1991). Moulton & Feigelson (1991) reexamined the partial phase diagram of the PbF_2–AlF_3 system in the composition range 50–100 mol% PbF_2 for comparison with the earlier results of Shore & Wanklyn (1969). They established the existence both of $Pb_3Al_2F_{12}$ and a composition with approximately 63.5 mol% PbF_2; $Pb_5Al_3F_{19}$ contains 62.5 mol% PbF_2. $Pb_5Al_3F_{19}$ has been shown to form a continuous series of solid solutions with $Pb_5Cr_3F_{19}$, the low-temperature phase of which remains ferroelectric throughout the entire composition range (Ravez, Simon, Andriamampianina, Grannec, Hagenmuller & Abrahams, 1990). The composition $Pb_5Al_3F_{19}$ is found to undergo three different phase transitions on cooling from 400 to 80 K (Ravez, Andriamampianina, Simon, Rabardel, Ihringer & Abrahams, 1994), with a lattice-parameter thermal dependence over the range 50–397 K that has been determined by Ihringer, Ravez & Abrahams (1994). The space group of the antiferroelectric phase is *P*4/*n*; the structure of this phase at 295 K has been reported by Andriamampianina, Gravereau, Ravez & Abrahams (1994), who also discussed the structural relationship between it and ferroelectric $Pb_5Cr_3F_{19}$. The antiferroelectric phase of $Pb_5Al_3F_{19}$ undergoes a first-order transition to the ferroelectric phase at 120 K on cooling (Ihringer *et al.*, 1994). The reverse transition on heating from the ferroelectric to the antiferroelectric phase takes place at 270 K. Since a clearer understanding of this phase change in $Pb_5Al_3F_{19}$ may be expected from an examination of the atomic displacements that occur on cooling through the phase-transition temperature, it was necessary to determine the structure of ferroelectric $Pb_5Al_3F_{19}$ as presented below.

2. Experimental

The crystals used in the structural investigations were grown by the method described in detail by

Table 1. *Fractional atomic coordinates and equivalent isotropic displacement parameters ($Å^2$) for $Pb_5Al_3F_{19}$ at 160 K*

$$U_{eq} = (1/3)\Sigma_i\Sigma_j U_{ij} a_i^* a_j^* \mathbf{a}_i.\mathbf{a}_j.$$

	x	y	z	U_{eq}
Pb1	0.42602 (4)	0.27489 (4)	0†	0.011 (2)
Pb2	0	0.50000	0.1350 (3)	0.018 (1)
Al1	0.1628 (4)	0.3372	−0.021 (1)	0.008 (3)
Al2	0	0	0.188 (2)	0.009 (1)
F1	0.1140 (10)	0.2478 (9)	−0.174 (2)	0.017 (2)
F2	0.1970 (10)	0.4294 (8)	0.142 (2)	0.014 (1)
F3	0.0761 (6)	0.4239	−0.097 (3)	0.016 (2)
F4	0.2479 (7)	0.2521	0.069 (3)	0.015 (1)
F5	0	0	0.438 (2)	0.027 (8)
F6	−0.0540 (10)	0.1175 (6)	0.673 (2)	0.016 (2)
F7	0.3835 (8)	0.1165	0.021 (4)	0.010 (5)

† Origin. Parameters without uncertainties are derived or are at special positions.

Andriamampianina *et al.* (1994). Both structure-factor intensity distribution and Rietveld analysis of the powder diffraction profile led to the limiting diffraction conditions $h + k + l = 2n$ and $k, l = 2n$ for hkl and $0kl$ reflections, respectively. Possible space groups are hence $I\bar{4}c2$, $I4/mcm$ or $I4cm$. The unambiguous detection of both pyroelectric and piezoelectric responses, see below, eliminated $I\bar{4}c2$ and $I4/mcm$. The sphere used for intensity measurement was ground by pulsed-air flow around a race lined with 600 μm grit, see Table 2. The sphere was initially cooled to 77 K, then heated to 160 K using a dry nitrogen gas stream. The maximum thermal variation at the sphere during the diffraction measurements was *ca* 1 K. The structure clearly resembled that of ferroelectric $Pb_5Cr_3F_{19}$ (Abrahams, Albertsson, Svensson & Ravez, 1990) and substitution of Al for Cr in the coordinates of that structure led to a successful solution. Following the refinement of isotropic displacement parameters for all atoms, each was varied anisotropically. Reversal of the polarization direction and subsequent refinement increased the value of wR significantly to 0.0554. The final atomic coordinates are given in Table 1. All other crystal data, data collection variables and refinement parameters are presented in Table 2.* The locally written program for calculating interatomic distances and uncertainties did not use the full variance–covariance matrix, hence the given uncertainties may be underestimated.

The larger crystals used for pyroelectric and piezoelectric measurements were grown by an inverted Bridgman-like technique using a covered cylindrical graphite crucible and a melt composition of 60% PbF_2–40% AlF_3, with liquidus temperature around 1025 K. The material melts incongruently at 922 K and therefore crystals can only be grown from a PbF_2-rich solution below the peritectic decomposition temperature. The inverted technique (growth from the top down) was chosen because AlF_3, the first phase to solidify from a

Table 2. *Crystal data, data collection and refinement parameters for $Pb_5Al_3F_{19}$ at 160 K*

Crystal data	
Chemical formula	$Pb_5Al_3F_{19}$
Chemical formula weight	1477.9
Cell setting	Tetragonal
Space group	*I4cm*
a (Å)	14.07 (2)
c (Å)	7.30 (1)
V ($Å^3$)	1445 (3)
Z	4
D_x (Mg m^{-3})	6.793
D_m (Mg m^{-3})	6.66 (1) at 295 K
D_m measured by	Pycnometry at 295 K
$F(000)$	2480
Radiation type	Mo $K\alpha$
Wavelength (Å)	0.71073
No. of reflections for cell parameters	25
θ range (°)	9.0–22.0
μ (mm^{-1})	56.36
Temperature (K)	160 (1)
Crystal form	Sphere
Crystal radius (mm)	0.27 (1)
Crystal color	Colorless
Data collection	
Diffractometer	Enraf–Nonius CAD-4
Data collection method	$\omega/2\theta$ [width $(3.0 + 2.5\tan\theta)°$]
Absorption correction	Spherical
T_{min}	0.0009
T_{max}	0.0246
No. of measured reflections	4180
No. of independent reflections	742
No. of observed reflections	656
Criterion for observed reflections	$I > 3\sigma(I)$
R_{int}	0.077
θ_{max} (°)	60
Range of h, k, l	$-29 \rightarrow h \rightarrow 29$ $0 \rightarrow k \rightarrow 29$ $0 \rightarrow l \rightarrow 16$
No. of standard reflections	3
Frequency of standard reflections (min)	120
Intensity decay (%)	<5
Refinement	
Refinement on	F
R	0.0527
wR	0.0480
S	1.065
No. of reflections used in refinement	656
No. of parameters used	71
Weighting scheme	$w = [1/\sigma^2(F)]\{1 - [(F_o - F_c)/6\sigma(F)]^2\}^2$
$(\Delta/\sigma)_{max}$	0.14
$\Delta\rho_{max}$ (e $Å^{-3}$)	5
$\Delta\rho_{min}$ (e $Å^{-3}$)	−6
Extinction method	Secondary (Larson, 1970)
Extinction coefficient	g = 31.1 (11)
Source of atomic scattering factors	Cromer & Waber (1974)
Computer programs	
Data collection	*CAD-4 Software* (Enraf–Nonius, 1989)
Cell refinement	*CAD-4 Software*
Data reduction	Local program (unpublished)
Structure refinement	*CRYSTALS* (Watkin, Carruthers & Betteridge, 1985)

* Lists of structure factors, anisotropic atomic displacement parameters for all atoms and bond angles in the Pb and Al atom polyhedra have been deposited with the IUCr (Reference: MD0001). Copies may be obtained through The Managing Editor, International Union of Crystallography, 5 Abbey Square, Chester CH1 2HU, England.

melt of this composition, has a density much lower than that of the melt. The regular Bridgman technique leads to homogenization and gravity-driven segregation problems, with subsequent poor crystal quality. The initial nucleation, by several grains, took place at the free melt surface and these were grown downward by raising the crucible in the furnace at a rate of $0.5\,mm\,h^{-1}$ through a thermal gradient of $\sim 2.5\,K\,mm^{-1}$ at the growth temperature. Starting materials were presynthesized and purified in an HF–Ar atmosphere to minimize OH^- and O_2 contamination.

3. Pyroelectric and piezoelectric measurements and results

Pyroelectric measurements were made on an 0.14 mm thick (001) single-crystal plate with surface area of $1.23\,mm^2$. Silver wires attached to each surface, electroded with silver paste, allowed the crystal to be suspended in a stainless-steel cell filled with dry helium. The wires were connected to a Keithley 610C electrometer and recorder. The plate was slowly cooled to 77 K, then heated at a constant rate of $5\,K\,min^{-1}$. Numerous pyroelectric pulses, of the order 10^{-2} K in width and $2200\,\mu C\,m^{-2}\,K^{-1}$ in magnitude and primarily of one sign, but with many smaller pulses of opposite sign, were recorded as the plate temperature rose from 77 to 200 K. Sign reversals are attributed to domains of opposite orientation in the largely single domain plate. Application of a $700\,kV\,m^{-1}$ electric field while cooling from 120 to 80 K had no effect upon the pyroelectric pulse distribution. Such pyroelectric currents are produced only from 120 K on cooling and thereafter to 270 K on heating.

Piezoelectric interactions were detected by observing the electrical impedance frequency dependence of a silver paste-electroded crystal prism with dimensions 2 mm along the z axis and 2.9×4.2 mm along the x_1 and x_2 axes, respectively. The prism was suspended by silver wires in the same cell used for the pyroelectric measurements and was connected to an HP4194A impedance bridge under microcomputer control. The prism was slowly cooled to 98 K. Numerous piezoelectric resonances with widths of the order 10 kHz, absent at 295 K, were reproducibly observable between 650 and 1200 kHz at 98 K in the polar *4mm* phase. A piezoelectric resonance corresponding to a compression mode along 0z has been isolated at ~ 1197 kHz, as demonstrated by the admittance circle shown in Fig. 1. Vector admittance circles are used to estimate characteristic frequencies required for evaluating equivalent circuit parameters.

The mechanical quality factor $Q_m = |X|/R$, where X is the reactance or imaginary part of the impedance and R is the resistance or real part of the impedance, may be calculated from the expression $Q_m = 1/2\pi RCf_r$, given by Berlincourt, Curran & Jaffe (1964), as ~ 423. In the equivalent piezoelectric circuit used, $R = 7.86 \times 10^6\,\Omega$, $C = 4.00 \times 10^{-17}$ F and $f_r = 1197.06$ kHz. Comparable values reported for Q_m are 300 for $BaTiO_3$ (Berlincourt, 1971), 543 for $PbZr_{0.448}Ti_{0.552}O_3$ (Weston, Webster & McNamara, 1967) and 1000 for $Pb_{0.4}Ba_{0.6}Nb_2O_6$ (Baxter & Hellicar, 1960).

4. Structure at 160 K

The structure of ferroelectric $Pb_5Al_3F_{19}$ contains infinite chains of corner-sharing AlF_6 octahedra, individual AlF_6 octahedra, individual F^- ions and polyhedrally F-atom-coordinated Pb^{2+} ions. A view along the polar axis of the content of a unit cell is presented in Fig. 2 and that along the a_2 axis in Fig. 3. The average Al—F distances in the Al1 and Al2 octahedra are 1.818 (5) and 1.824 (1) Å, respectively (Table 3). Pb1 has nine nearest F-atom neighbors, with an average Pb—F distance of 2.66 (22) Å, Pb2 is ten coordinated, with an average Pb—F distance of 2.61 (28) Å. These distances may be compared with the five independent average PbF_n polyhedral distances found by Andriamampianina *et al.* (1994) in the antiferroelectric phase that range from 2.66 (15) to 2.72 (17) Å for $n = 9$, 10 and the four independent average Al—F distances in the AlF_6 octahedra that range from 1.750 (30) to 1.850 (42) Å.

$Pb1F_9$ may be described as a distorted tricapped trigonal prism, with F1, F4, F7 in the lower scalene (with respect to the positive c axis), F1, F6, F6 in the upper scalene and F2, F6 capping faces with F2 capping an edge, see Fig. 4(*a*). $Pb2F_{10}$ may be described as a bicapped diagonally compressed cuboid with four F2, two F3 and two F7 atoms at the vertices and two F3 as capping atoms, see Fig. 4(*b*), in which there are two short Pb2—F3, two medium Pb2—F3, two medium Pb2—F7 and four long Pb2—F2 bonds. A similar polyhedral

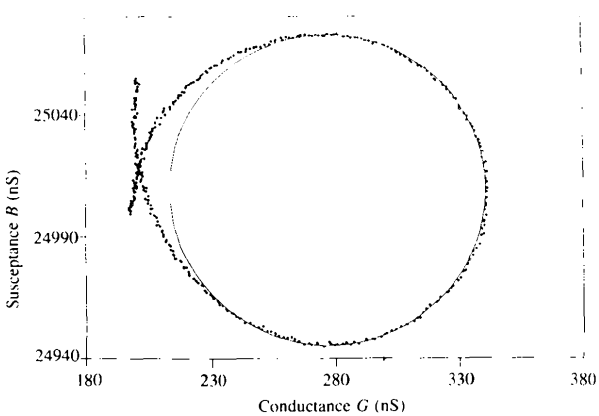

Fig. 1. Admittance circle for the [001] compression mode at 1197 kHz in $Pb_5Al_3F_{19}$ at 98 K. B is the susceptance or imaginary part of the admittance, G is the conductance for direct current or real part of the admittance ($G = 1/R$, where R is the resistance). The units of each are in siemens ($1\,S = 1\,A\,V^{-1}$). The points represent experimental values, the continuous line a best-fit circle as a visual aid.

Table 3. *Coordination distances (Å) in $Pb_5Al_3F_{19}$ at 160 K*

Pb1—F7	2.31 (2)	Pb2—F3^{i}	2.27 (3) × 2
—F1$_1$	2.47 (1)	—F7^{ii}	2.46 (2) × 2
—F2$_2$	2.53 (1)	—F3^{iii}	2.48 (2) × 2
—F4	2.58 (2)	—F2^{iv}	2.93 (1)* × 4
—F6$_3$	2.67 (2)		
—F6$_4$	2.78 (2)		
—F2$_5$	2.83 (1)		
—F6$_6$	2.84 (2)		
—F1$_7$	2.95 (1)*		
Al1—F3	1.810 (9)	Al2—F6^{vi}	1.823 (5) × 4
—F1^{v}	1.816 (6) × 2	—F5^{vii}	1.825 (7) × 2
—F4	1.818 (9)		
—F2^{v}	1.824 (6) × 2		

Symmetry codes: (1) $\frac{1}{2}-x,\frac{1}{2}-y,\frac{1}{2}+z$; (2) $1-y,x,z$; (3) $\frac{1}{2}-x,\frac{1}{2}-y,z-\frac{1}{2}$; (4) $\frac{1}{2}-y,\frac{1}{2}+x,z-\frac{1}{2}$; (5) $y,x,z-\frac{1}{2}$; (6) $\frac{1}{2}+x,\frac{1}{2}-y,z-1$; (7) $\frac{1}{2}+x,\frac{1}{2}-y,z$; (8) $-x,1-y,z$; (9) $x-\frac{1}{2},\frac{1}{2}-y,z$; (10) $\frac{1}{2}-x,\frac{1}{2}+y,z$; (11) $x,1-y,\frac{1}{2}+z$; (12) $-x,y,\frac{1}{2}+z$; (13) $\frac{1}{2}-y,\frac{1}{2}-x,z$; (14) $y-\frac{1}{2},\frac{1}{2}+x,z$; (15) $\frac{1}{2}+y,\frac{1}{2}+x,z$; (16) $-y,-x,z-\frac{1}{2}$; (17) $y,x,z-\frac{1}{2}$; (18) $x,-y,z-\frac{1}{2}$; (19) $-x,y,z-\frac{1}{2}$. No symmetry code implies the coordinates in Table 1. Superscripts on atoms forming multiple bonds refer to the following symmetry codes, in addition to the basic *xyz* coordinates of Table 1 where applicable: (i) 8; (ii) 9, 10; (iii) 11, 12; (iv) 8, 13, 14; (v) 13; (vi) 16, 17, 18, 19: (vii) 19. *Next largest Pb1—F distance is 3.17 (1) Å, next largest Pb2—F distance is 3.65 (1) Å.

shape was reported for $Pb3F_{10}$ in the antiferroelectric phase of $Pb_5Al_3F_{19}$ (Andriamampianina *et al.*, 1994). The Pb-atom lone-electron pair is expected to be a major cause of the PbF_n polyhedral distortions. A reduction in Pb—F bond length is also expected if the bond is overlapped by the lone pair; it may be noted that the shortest bonds are Pb1—F7 (at 2.31 Å) and Pb2—F3 (at 2.27 Å), each of which may hence be close to a lone-pair direction.

It is notable that the direction of the major displacement-ellipsoid axis for each F atom in both independent AlF_6 octahedra is approximately normal to the corresponding Al—F direction, as observed along the polar direction, indicative of a major oscillatory displacement mode by each octahedron about its central Al atom.

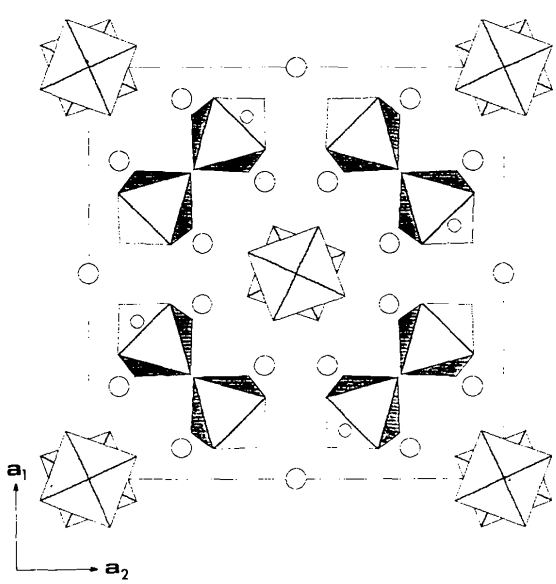

Fig. 2. Projection of the structure of ferroelectric $Pb_5Al_3F_{19}$ at 160 K along the polar *c* axis. The AlF_6 octahedra are shown shaded; closest pairs of Al(2)F_6 octahedra are related by twofold screw axes between pairs. The larger filled circles represent Pb and the smaller open circles F7 atoms.

5. Structural reversal of spontaneous polarization

The model used by Abrahams *et al.* (1990) for calculating the atomic displacements required in ferroelectric $Pb_5Cr_5F_{19}$ in order to become paraelectric may be followed for ferroelectric $Pb_5Al_3F_{19}$. A shift in origin along the polar axis by 0.0415 would result in equal but opposite sense displacements of 0.150 Å by Al1 and Al2 to the special planes at $z=0$ and $\frac{1}{4}$. Any other choice of origin necessarily increases Al(Δz) for one or other of the independent Al atoms. However, since the effective mean *z* coordinate of each fluorine octahedron must also be considered, see below, an origin shift of 0.0437 is used in Table 4 to give the two independent octahedral centers equal but opposite displacements from the special planes; the displacement by Al1 hence increases slightly, that by Al2 decreases. The Wyckoff position for each atom in space group *I4cm* is listed in Table 4 together with the corresponding *z'* coordinate with respect to the new origin, the *z''* coordinate in the hypothetical paraelectric space group *I4/mcm* and the magnitude of each atomic displacement from its respective *z''* coordinate. Additional displacements from the *x* and *y* coordinates of F1 and F2 given in Table 1 are necessary in order for these two atoms to become equivalent and occupy Wyckoff position 32(*m*) in the hypothetical paraelectric space group.

The 0.0437 origin shift results in no value of $\Delta z > 0.83$ Å, within the range expected for ferroelectric

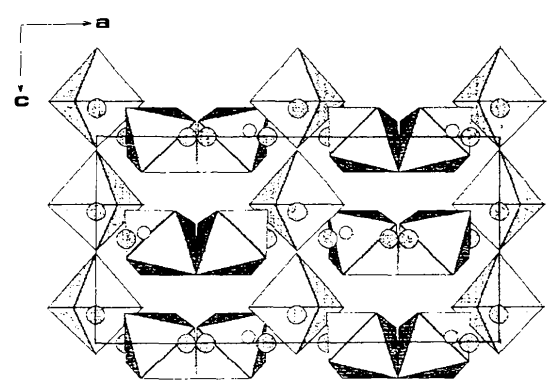

Fig. 3. Projection of the structure of ferroelectric $Pb_5Al_3F_{19}$ at 160 K along the polar a_2 axis, with octahedra and circles represented as in Fig. 2.

crystals (Abrahams, 1988). An atomic arrangement in which the z'' coordinates of Table 4 replace the experimental z coordinates could, in principle, undergo with equal probability atomic movements in which the signs of all Δz displacements are reversed, thereby reversing the spontaneous polarization as required for a demonstration of structural ferroelectricity. The temperature at which the structure at 160 K transforms to space group $I4/mcm$ may be estimated from relationship (1) given by Abrahams, Kurtz & Jamieson (1968)

$$T_c = (\mathcal{K}/2k)(\Delta z)^2 \text{ K}, \quad (1)$$

where $\mathcal{K}$ is a force constant and k is Boltzmann's constant with $\mathcal{K}/2k = 2.00(9) \times 10^4$ K Å^{-2}. It is necessary to take not only the polar displacements by the Al atoms into account in (1) but also those of each related octahedron of F atoms. In the case of Al1 a displacement of 0.042 Å, and for Al2 a displacement of 0.073 Å, must hence be added to the displacements given under Δz in Table 4. The final resulting $\Delta z(\text{Al1}) = \Delta z(\text{Al2}) = 0.207(28)$ Å leads to a predicted $T_c = 860(230)$ K; the large uncertainty is caused primarily by the difficulty in accurately determining F-atom positions in the presence of Pb using X-ray diffraction. The spontaneous polarization P_s may also be calculated as 0.53 (2) C m^{-2} from relationship (2) given by Abrahams *et al.* (1968)

$$P_s = 258(9) \times 10^{-2} \Delta z \text{ C m}^{-2}. \quad (2)$$

The transition on heating at 260 K is from the ferroelectric to the antiferroelectric phase with space group $P4/n$ (Andriamampianina *et al.*, 1994). It is of considerable interest to establish whether the intervention of this and at least two other phase transitions before reaching the paraelectric phase at higher temperatures (Ravez, Andriamampianina & Abrahams, 1994) affects the validity of the predicted Curie temperature.

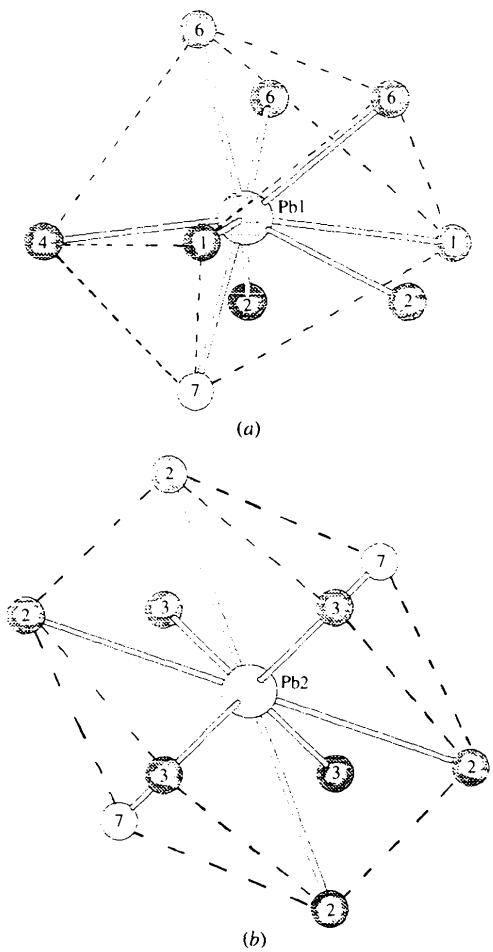

(*a*)

(*b*)

Fig. 4. (*a*) Distorted tricapped trigonal prism of F atoms in the $Pb1F_9$ polyhedron. (*b*) Distorted bicapped diagonally compressed cuboid of F atoms in the $Pb2F_{10}$ polyhedron.

Table 4. *Polar coordinates and atomic displacements required for $Pb_5Al_3F_{19}$ at 160 K to become paraelectric*

$\Delta z = (z' - z'')c$, where $z' = z + 0.0437$ and z'' is the coordinate value in the hypothetical paraelectric state. The xyz coordinates are given in Table 2.

	Wyckoff position	z'	z''	Δz (Å)
Pb1	16(*d*)	0.0437	0	0.319
Pb2	4(*b*)	0.1787	0.25	−0.520
Al1	8(*c*)	0.0277	0	0.166
Al2	4(*a*)	0.2317	0.25	−0.134
F1	16(*d*)	−0.1303	−0.158	0.202
F2	16(*d*)	0.1857	0.158	0.202
F3	8(*c*)	−0.0533	0	−0.389
F4	8(*c*)	0.1127	0	0.823
F5	4(*c*)	0.4817	0.5	−0.134
F6	16(*d*)	0.7167	0.75	−0.243
F7	8(*c*)	0.0647	0	0.472

6. Relationship of ferroelectric $Pb_5Al_3F_{19}$ at 160 K to ferroelectric $Pb_5Cr_3F_{19}$ at 295 K

The atomic coordinates of ferroelectric $Pb_5Al_3F_{19}$ at 160 K in Table 1 are very similar to those of ferroelectric $Pb_5Cr_3F_{19}$ at 295 K. A detailed comparison is provided in Table 5, which lists the differences between corresponding coordinates, taking the origin along the polar axis at Pb1. It is notable that a difference in z coordinate as large as 0.08 Å is found between Cr1 and Al1, with a largest difference of 0.17 Å found between the z(F2) coordinates in the two materials. Several x and y coordinates also differ as much as 0.08 Å. The expected dipole–dipole interaction between the Pb^{2+} lone pair of electrons and the spin moment (for $0 < n < 10$) of the n $3d$ electrons at the $M^{3+}F_6$ octahedra, with M = Al, Ti, V, Cr, Fe or Ga (Ravez, Andriamampianina, Simon *et al.*, 1994), is scarcely revealed by the octahedral orientational differences between $M = \text{Al}(n = 0)$ and $\text{Cr}(n = 5)$. Individual octahedra may rotate both in the (110) and parallel to the (001) planes; the ($M1F_6$) octahedra differ by rotations of 3.0° in the former (F4, Al1, F3) and by 2.0° in the latter plane (F1, Al1 and F2). Corner-sharing

Table 5. *Differences (Å) between corresponding atomic coordinates in ferroelectric $Pb_5Cr_3F_{19}$ at 295 K and ferroelectric $Pb_5Al_3F_{19}$ at 160 K*

Four atoms in the 1990 list of $Pb_5Cr_3F_{19}$ atomic coordinates are renumbered below, from F3 to F6, F5 to F7, F6 to F3 and F7 to F5.

$\langle a \rangle = 14.227$, $\langle c \rangle = 7.354$ Å.

	Δx	Δy	Δz
Pb1	0.005	−0.031	0
Pb2	0	0	0.116
Cr1, Al1	0.006	−0.006	0.076
Cr2, Al2	0	0	−0.060
F1	−0.078	0.014	0.010
F2	0.020	0.021	0.172
F3	−0.058	0.058	0.104
F4	0.063	−0.063	−0.088
F5	0	0	−0.042
F6	−0.041	−0.031	0.107
F7	0.030	−0.030	−0.011

octahedra may rotate only in the *ab* plane; the angular difference between octahedra with *M*2 either Al or Cr is only 3.2° in this plane. It is noted that the two shortest Pb—F distances, expected to approximate the direction of the lead lone-electron pair, are Pb1—F7 and Pb2—F3; only the latter is directly bonded to an AlF_6 octahedron and may influence its orientation strongly.

7. Transition from ferroelectric to antiferroelectric phase

The relationship between the structures of ferroelectric $Pb_5Cr_3F_{19}$ at 295 K and antiferroelectric $Pb_5Al_3F_{19}$, also at 295 K, have been considered in detail by Andriamampianina *et al.* (1994). The origin of the first-order transition between the ferroelectric and antiferroelectric phases in $Pb_5Al_3F_{19}$ is clearly associated with the orientational change from an eclipsed arrangement of AlF_6 octahedra along the inversion and rotation-tetrad axes in the latter to a staggered arrangement of AlF_6 octahedra along the rotation-tetrad axes in the former phase. The close structural similarity (see Table 5) between ferroelectric $Pb_5Cr_5F_{19}$ and ferroelectric $Pb_5Al_3F_{19}$ confirms this association. A more detailed consideration of the structural changes at this and all other phase transitions in $Pb_5Al_3F_{19}$ will be presented following completion of the structure refinement of each.

References

Abrahams, S. C. (1988). *Acta Cryst.* B**44**, 585–595.

Abrahams, S. C. & Ravez, J. (1992). *Ferroelectrics*, **135**, 21–37.

Abrahams, S. C., Albertsson, J., Svensson, C. & Ravez, J. (1990). *Acta Cryst.* B**46**, 497–502.

Abrahams, S. C., Kurtz, S. K. & Jamieson, P. B. (1968). *Phys. Rev.* **87**, 551–553.

Andriamampianina, V., Gravereau, P., Ravez, J. & Abrahams, S. C. (1994). *Acta Cryst.* B**50**, 135–141.

Baxter, P. & Hellicar, N. J. (1960). *J. Am. Ceram. Soc.* **43**, 578–583.

Berlincourt, D. A. (1971). *Ultrasonic Transducer Materials*, edited by O. Mattiat, pp. 63–124. New York: Plenum Press.

Berlincourt, D. A., Curran, D. R. & Jaffe, H. (1964). *Physical Acoustics*, edited by W. P. Mason, pp. 169–270. New York: Academic Press.

Cromer, D. T. & Waber, J. T. (1974). *International Tables for X-ray Crystallography*, Vol. IV, Tables 2.2A and 2.3.1. Birmingham: Kynoch Press. (Present distributor Kluwer Academic Publishers, Dordrecht.)

Enraf–Nonius (1989). *CAD-4 Software*. Version 5.0. Enraf–Nonius, Delft, The Netherlands.

Ihringer, J., Ravez, J. & Abrahams, S. C. (1994). *Z. Kristallogr.* **210**, 853–857.

Larson, A. C. (1970). *Crystallographic Computing*, edited by F. R. Ahmed, pp. 291–294, equation (22). Copenhagen: Munksgaard.

Moulton, L. V. & Feigelson, R. S. (1991). *J. Mater. Res.* **6**, 2188–2192.

Ravez, J. (1985). *Inorganic Solid Fluorides*, pp. 469–475. London: Academic Press.

Ravez, J. (1986). *Rev. Chim. Miner.* **23**, 460–473.

Ravez, J., Andriamampianina, V. & Abrahams, S. C. (1994). *Ferroelectrics*, **158**, 133–137.

Ravez, J., Andriamampianina, V., Simon, A., Grannec, J. & Abrahams, S. C. (1991). *J. Appl. Phys.* **70**, 1331–1336.

Ravez, J., Andriamampianina, V., Simon, A., Rabardel, L., Ihringer, J. & Abrahams, S. C. (1994). *J. Appl. Cryst.* **27**, 362–368.

Ravez, J., Simon, A., Andriamampianina, V., Grannec, J., Hagenmuller, P. & Abrahams, S. C. (1990). *J. Appl. Phys.* **68**, 3529–3531.

Shore, R. G. & Wanklyn, B. M. (1969). *J. Am. Ceram. Soc.* **52**, 79–81.

Watkin, D. J., Carruthers, J. R. & Betteridge, P. W. (1985). *CRYSTALS User Guide*. Chemical Crystallography Laboratory, University of Oxford, England.

Weston, B., Webster, A. M. & McNamara, V. N. (1967). *J. Can. Ceram. Soc.* **36**, 15–20.